Macromolecules

pubs.acs.org/Macromolecules Article

Equilibrium Melting Temperature Depression in Syndiotactic Poly(styrene-*stat*-3-methylstyrene) and Poly(styrene-*stat*-4-methylstyrene)

Po-Hsun Chen,* Shi-Jie Lin, Jing-Cherng Tsai, U-Ser Jeng, and An-Chung Su*

Cite This: *Macromolecules* 2020, 53, 3059−3070 Read Online

ACCESS | Metrics & More | Article Recommendations | Supporting Information

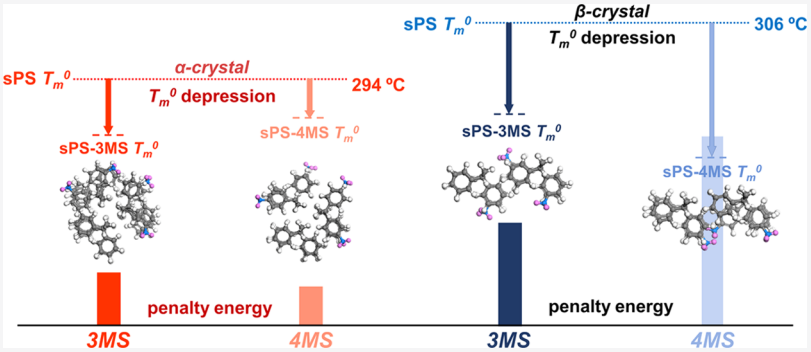

ABSTRACT: After randomly incorporating 2−21 mol % of 3-methylstyrene (3MS) or 4-methylstyrene (4MS) into the syndiotactic polystyrene (sPS) backbone, the effects of the comonomer units on the equilibrium melting temperature (T_m°) depression were examined within the Sanchez−Eby theoretical framework. In situ small-/wide-angle X-ray scattering (SAXS/WAXS) was used to investigate the morphological evolution upon heating. The WAXS profiles showed that the α- or β-dominated crystals in syndiotactic poly(styrene-*stat*-3-methylstyrene) (sPS-3MS) and poly(styrene-*stat*-4-methylstyrene) (sPS-4MS) all consistently reach complete melting with no signs of interphase transformation. By analyzing the corresponding SAXS heating profiles with a polyradius cylinder form factor, the correlations between the crystal thickness (l_c) and temperature were identified; the corresponding T_m° value was then determined via constructing the Gibbs−Thomson melting line and extrapolating it to the infinite crystal thickness. Generally, the T_m° of α and β crystals decreases with increasing comonomer content, and the T_m° for the β phase was always higher than that of the α counterpart. The level of T_m° depression was interpreted in terms of the Sanchez−Eby theory, showing that the introduction of methyl groups into the β structure has higher penalty energy than that into the α structure in both sPS-3MS and sPS-4MS cases, suggesting that incorporating the methyl groups more significantly destabilizes the β crystals and leads to a further preference for α crystal formation. Comparing the β crystals between sPS-3MS and sPS-4MS systems, the penalty energy for incorporating 4MS units into the β lattice is greater than that in the 3MS case; for the α crystals, the penalty energy for incorporating 3MS units is greater than that in the 4MS case.

Downloaded via SYNCHROTRON RADIATION RESEARCH on January 27, 2021 at 03:21:17 (UTC).
See https://pubs.acs.org/sharingguidelines for options on how to legitimately share published articles.

INTRODUCTION

The equilibrium melting temperature (T_m°) of a crystallizable polymer is defined as the melting temperature of the infinitely thick crystal ($l_c \rightarrow \infty$), representing the equilibrium between the idealized polymer solid (free of the fold surface) and the corresponding melt. The T_m° is a crucial thermodynamic property for polymers, which acts as the reference temperature for defining the degree of supercooling, i.e., the driving force of crystallization. After randomly introducing the comonomer units (B) into the crystallizable homopolymer (A), the melting temperature is depressed along with the crystallization temperature range. For random copolymers, the distribution of comonomer units in the crystalline structure may lie between two extremes. At one extreme, the comonomer units are fully excluded from the crystalline structure, raising the concentration of comonomer units in the amorphous phase; at the other extreme, the comonomer units are nondiscriminatingly incorporated into the crystalline lattice, resulting in a uniform composition in the crystalline and amorphous phases.[1] In 1955, Flory developed the equilibrium melting temperature of random copolymers where noncrystallizable comonomer B units are fully excluded from the crystalline structure.[2] The

Received: September 1, 2019
Revised: March 29, 2020
Published: April 10, 2020

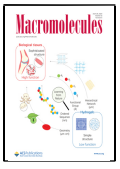

© 2020 American Chemical Society

https://dx.doi.org/10.1021/acs.macromol.9b01831
Macromolecules 2020, 53, 3059−3070

equilibrium melting temperature depression was then related to the probability that a crystallizable A segment is connected to another A segment, which is independent of the comonomer type

$$\frac{1}{T_m^\circ(x)} - \frac{1}{T_m^\circ} = \frac{R}{\Delta H_m^\circ}[-\ln(1-x)] \quad (1)$$

where $T_m^\circ(x)$ is the equilibrium melting temperature for the random copolymer, T_m° and ΔH_m° are the equilibrium melting temperature and the heat of fusion of the perfect crystal for the homopolymer, respectively, R is the gas constant, and x is the mole fraction of noncrystallizable B units in the copolymer chain. Previous studies on polyethylene (PE)-based random copolymers[3−5] showed that the relation between experimentally determined melting temperature $T_m(x)$ and x among several comonomer types can be described by a single master curve, supporting Flory's prediction that the melting temperature depression is independent of the comonomer type. However, as shown by Richardson et al.,[3] the master curve was parallel-shifted to lower temperatures when the comonomer structure was changed from methyl to ethyl and *n*-propyl groups, implying different levels of comonomer unit exclusion in the PE lattice. In addition, later studies showed that eq 1 tends to underestimate the melting temperature depression.[6−14]

Apart from the fully excluded case, Sanchez and Eby[1] derived a general equation to describe T_m° depression of random copolymers where noncrystallizable B units can either be excluded from the crystalline structure or incorporated into the crystalline structure as the defects

$$\frac{1}{T_m^\circ(x)} - \frac{1}{T_m^\circ} = \frac{R}{\Delta H_m^\circ}\left[\frac{\varepsilon x_c}{RT_m^\circ(x)} + (1-x_c)\ln\left(\frac{1-x_c}{1-x}\right) + x_c\ln\left(\frac{x_c}{x}\right)\right] \quad (2)$$

in which the concentration of noncrystallizable B units in the crystal (x_c) and the "penalty energy" ε (which describes the crystalline energy increase after incorporating the comonomer units as the defects in the structure) are two key parameters. The comonomer units are assumed to be randomly incorporated into the crystal and do not have interaction with each other; hence, the penalty energy may be described by a mean value.[14] The first term in the bracket is the enthalpic contribution, and the other logarithmic terms are the entropic contribution to the free energy of mixing upon crystal melting. As the case of $x_c = 0$ corresponds to the full exclusion of the comonomer units from the crystalline phase, eq 2 reduces to eq 1.[1] Although the Sanchez−Eby model can generally describe the experimental results of melting temperature depression, discrepancies between the theoretical T_m° and experimental T_m° exist.[9,10,13−21] Martinez-Salazar et al.[15] use β and γ parameters (β is related to the x_c, and γ represents the penalty energy) to fit the experimental equilibrium melting temperatures determined via the Hoffmann−Weeks method for polyethylene-based random copolymers. Orts et al.[16] assumed that the β-hydroxyvalerate comonomer units were uniformly included in poly(β-hydroxybutyrate) crystals, and the results described the experimental differential scanning calorimetry (DSC) melting peak temperature well, while the corresponding penalty energy decreased with increasing comonomer content. Both Martinez-Salazar et al. and Orts et al. found that T_m° for a higher comonomer content case deviated from the theoretical prediction.[15,16] Kim et al.[17] used the Gibbs−Thomson equation to determine T_m° of ethylene−octene random copolymers and concluded that eq 1 described T_m° at lower comonomer contents, while eq 2 better predicted T_m° at higher comonomer levels, where ε decreases with increasing comonomer units. In subsequent studies,[14,18−21] the x_c is assumed to be in an equilibrium state, i.e., $x_c = x_{eq} = x\,e^{-\varepsilon/RT}/(1 - x + x\,e^{-\varepsilon/RT})$, but the prediction of eq 2 gave overestimated results compared with experimental T_m (determined by either DSC melting peak or Hoffman−Weeks method). Until now, the methodology for using eq 2 seems to lack consistency, while apparent discrepancies between theoretical and experimental results exist; a systematic approach to determine reasonable T_m°, ε, and x_c is needed.

To have a better understanding of the comonomer effect on the melting temperature depression, a reliable T_m° determination is a priori. Strobl et al.[7,22−26] determined the relationship between the crystal thickness (l_c) and the melting temperature (T_m) using time- and temperature-dependent small-angle X-ray scattering (SAXS), and this relation can be described by the Gibbs−Thomson equation

$$T_m = T_m^\circ\left[1 - \frac{2\sigma_e}{\Delta H_m^\circ l_c}\right] \quad (3)$$

where σ_e is the fold surface energy. The melting line in the Gibbs−Thomson theory describes the thickness dependence of the phase transition from the crystal to liquid states; after extrapolating the melting line to the infinite thick case (where $l_c^{-1} = 0$), this temperature gives the equilibrium melting temperature.[27] Based on their time- and temperature-dependent SAXS results, Strobl et al. reported the equilibrium melting temperature for both the homopolymer[22−26] and the random copolymer[7,22,28] cases. For the comonomer-excluded cases of syndiotactic poly(propene-*co*-octene)s,[7,22] poly(ethylene-*co*-octene),[22,28] and poly(ethylene-*co*-butene),[28] they found that increasing the comonomer content leads to a parallel shift of the Gibbs−Thomson melting line to a lower temperature range, i.e., the slope of the melting line is independent of the comonomer content and consequently gives constant values of the fold surface energy.

Considering the thickness effect on the crystal melting, Sanchez and Eby also extended their general equation for the thin crystal case

$$\frac{1}{T_m^\circ(x)} - \frac{1}{T_m^\circ} = \frac{R}{\Delta H_m^\circ}\left[\frac{\varepsilon x_c}{RT_m^\circ(x)} + (1-x_c)\ln\left(\frac{1-x_c}{1-x}\right) + x_c\ln\left(\frac{x_c}{x}\right)\right] + \frac{2\sigma_e}{\Delta H_m^\circ l_c T_m^\circ(x)} \quad (4)$$

where the first bracket at the right side describes the T_m° depression as indicated in eq 2 and the second term at the right side describes the thickness dependence effect as indicated in eq 3.

In this report, on the basis of the method established by Strobl et al., we construct the melting lines for the α and β crystals of syndiotactic poly(styrene-*stat*-3-methylstyrene) (sPS-3MS) and poly(styrene-*stat*-4-methylstyrene) (sPS-4MS) random copolymers with different comonomer contents by analyzing in situ simultaneous synchrotron small-/wide-angle X-ray scattering (SAXS/WAXS) heating profiles. It is well known that syndiotactic polystyrene (sPS) has compli-

https://dx.doi.org/10.1021/acs.macromol.9b01831
Macromolecules 2020, 53, 3059−3070

cated polymorphism and its polymorphic behaviors have been extensively studied.[29−39] We have recently reported[40] the polymorphic results of sPS-3MS and sPS-4MS under bulk thermal treatment. Upon melt crystallization, sPS-3MS formed β-dominated crystals for 3MS content up to 11 mol %, followed by α-dominated crystals with a higher comonomer content (21 mol %); sPS-4MS only formed β-dominated crystals at 2 mol % 4MS content and gave α-dominated crystals at a higher 4MS level. Upon cold crystallization, sPS-3MS and sPS-4MS all consistently gave α crystals. (The α and β crystals can be further characterized into α', α'', β', and β'' submodifications by different degrees of structural order;[29−31,33] however, much more rigorous experimental design would be needed if considering these submodifications, and the comparision among these catagories would be more complicated (cf. SI α'' form in sPS-4MS). Thus, for the sake of simplicity, this report focuses on the difference between the general α and β crystals, which gives an intrinsic difference in the lattice packing.) Our results consistently show that the polymorphic behavior of sPS-3MS and sPS-4MS depends on the crystallization condition, while the presence of comonomer (especially 4MS) units tends to more strongly suppress the formation of β crystals in melt crystallization and the suppression level enhances with increasing comonomer content. (This agrees with the report from Manfredi et al.[41] that sPS-4MS with a higher 4MS content has stronger destabilization on the β crystal formation upon melt crystallization, while it appears to contradict the report from De Rosa et al.[42] that only sPS-3MS with 11 mol % content can form β crystals but give α crystals for copolymers with 4 and 21 mol % content upon melt crystallization. Furthermore, molecular mechanics calculations indicate that different steric repulsion levels (i.e., van der Waals interaction) for different amounts of 3MS or 4MS units within the crystal lattice indeed bear significance in α- and β-phase formation.[40]) Based on the experimentally constructed melting line, here the corresponding T_m° of the sPS α or β crystal with different 3MS and 4MS contents was determined and the Sanchez−Eby theory was introduced to interpret these observations from the viewpoint of thermodynamics.

EXPERIMENTAL DETAILS

Syndiotactic poly(styrene-*stat*-3-methylstyrene) (sPS-3MS, with 5−21 mol % 3MS units) and syndiotactic poly(styrene-*stat*-4-methylstyrene) (sPS-4MS, with 2−10 mol % 4MS units) specimens with weight-average molecular mass M_w = 125 ± 15 kDa, polydispersity index (PDI) = 2.5 ± 0.2, and high stereoregularity (>98% in the [rr] triad content), which were determined by gel permeation chromatography (GPC) and ^{1}H NMR (cf. experimental details in ref 40), were synthesized via established metallocene-catalyzed polymerization procedures.[43] Before use, all samples were purified via precipitation of hot *p*-xylene solutions in excess of methanol.

For both melt- and cold-crystallized thermal treatment, specimens were put into an INSTEC HCS 402 hot stage cell, which was controlled by an INSTEC mk1000 controller, and the protective nitrogen stream was introduced to prevent oxidation. For the melt crystallization process, specimens were first heated to 300 °C and kept for 3 min to erase the previous thermal history; after completely melted at 300 °C, these specimens were then quickly cooled to T_c (from 210 to 250 °C) for different periods of time before final quenching in liquid nitrogen. For the cold crystallization process, after keeping for 3 min at 300 °C, specimens were quenched in liquid nitrogen to obtain the amorphous glass, followed by isothermal treatment at T_c = 200−240 °C for various periods of time.

In situ simultaneous small-/wide-angle X-ray scattering (SAXS/WAXS) measurements were carried out at the Taiwan Light Source (TLS) beamline BL23A, National Synchrotron Radiation Research Center (NSRRC).[44] Specimens were sealed in punctured Al pans (ca. 0.7 mm in thickness and 6 mm in diameter) with Kapton windows for X-ray incident beam and use an INSTEC HCS302 sample holder as the temperature controller. With 10 keV beam (wavelength λ = 1.240 Å), in situ SAXS and WAXS data of sPS-3MS were collected, respectively, using a Pilatus 1M-F area detector (169 × 179 mm^2) and three Mythen-1K linear detectors (8 × 18 mm^2). The instrumental setup covered the SAXS q-range of 0.004−0.2 Å^{-1} and WAXS q-range of 0.75−1.7 Å^{-1}. For the sPS-4MS specimen, in situ SAXS and WAXS data were collected, respectively, using a Mar165 CCD detector of a 165 mm diameter active area and a flat panel C9728-DK area detector with 8 keV beam (λ = 1.55 Å). The scattering vector $q = 4\pi\lambda^{-1}\sin\theta$ (with 2θ being the scattering angle) was calibrated with silver behenate for SAXS and polyethylene and syndiotactic polystyrene for WAXS.

Data Analysis. SAXS profiles were modeled according to $I(q) = I_0P(q)S(q)$, where I_0 is the zero-angle scattering intensity, $P(q)$ is the normalized form factor that represents the shape contributions from the scattering objects, and $S(q)$ is the structure factor that represents the spatial arrangement contributions from the interparticle interferences. The scattering length density for amorphous sPS is 8.78×10^{-6} and 9.46×10^{-6} Å^{-2} for the sPS α-crystal and 9.85×10^{-6} Å^{-2} for the sPS β-crystal.

To construct the equilibrium melting line for sPS-3MS and sPS-4MS random copolymers, the thickness (l_c) of the nanograin needs to be determined. Generally, the thickness information can be extracted from the SAXS profile via a one-dimensional (1-D) correlation function, Kratky−Porod approximation, and form factor model fitting. The comparison among these methods is made and described in the Supporting Information (cf. SI Model for SAXS Analysis). After subtracting the molten state profiles (power-law scattering profile), these reduced SAXS profiles that approached melting were fitted with a cylinder shape form factor using a disperse radius model

$$P(q) = \frac{\text{scale}}{V_{\text{poly}}}\int_0^x f(r)\mathrm{d}r\int_0^{\pi/2} F^2(q,\alpha)\sin(\alpha)\mathrm{d}\alpha \tag{5}$$

where $f(r) = (z+1)^{z+1}x^z\{\exp[-(z+1)x]/r_{\text{avg}}\Gamma(z+1)\}$ is the normalized Schulz distribution of the radius (r), where z is related to the polydispersity ($p = \sigma/r_{\text{avg}}$) such that $z = 1/p^2 - 1$, σ^2 is the variance of the distribution, $x = r/r_{\text{avg}}$, and $\Gamma(x)$ is the γ function. The form factor calculation is normalized to the polydisperse volume using the second moment of radius distribution

$$V_{\text{poly}} = \pi r^2 L\left(\frac{z+2}{z+1}\right)$$

where L is the length of the cylinder, which is considered as the crystal thickness (l_c). $F(q,\alpha)$ is defined as

$$F(q,\alpha) = 2V_{\text{cyl}}(\rho_{\text{cyl}} - \rho_{\text{solv}})j_0(qH\cos\alpha)\frac{J_1(qr\sin\alpha)}{(qr\sin\alpha)}$$

where $V_{\text{cyl}} = \pi r^2 L$, $J_0(x) = \sin(x)/x$, $H = L/2$, α is the angle between the cylinder axis and the scattering vector q, and J_1 is the first-order Bessel function.[45]

The WAXS profiles were deconvoluted into Gaussian peaks combination using PeakFit software. The crystallinity (X_c) derived from the WAXS profile is defined as the peak area of crystalline reflection peaks over the total area

$$X_c = A_c/(A_c + A_a) \tag{6}$$

where A_c represents the area of crystalline reflection peaks and A_a represents the area of an amorphous halo. However, due to the limited q-range of the Mythen-1K linear detector, the full range of the WAXS profile cannot be collected; thus, in this report, the crystallinity represents the "relative crystallinity", meaning that areas of crystalline

https://dx.doi.org/10.1021/acs.macromol.9b01831
Macromolecules 2020, 53, 3059−3070

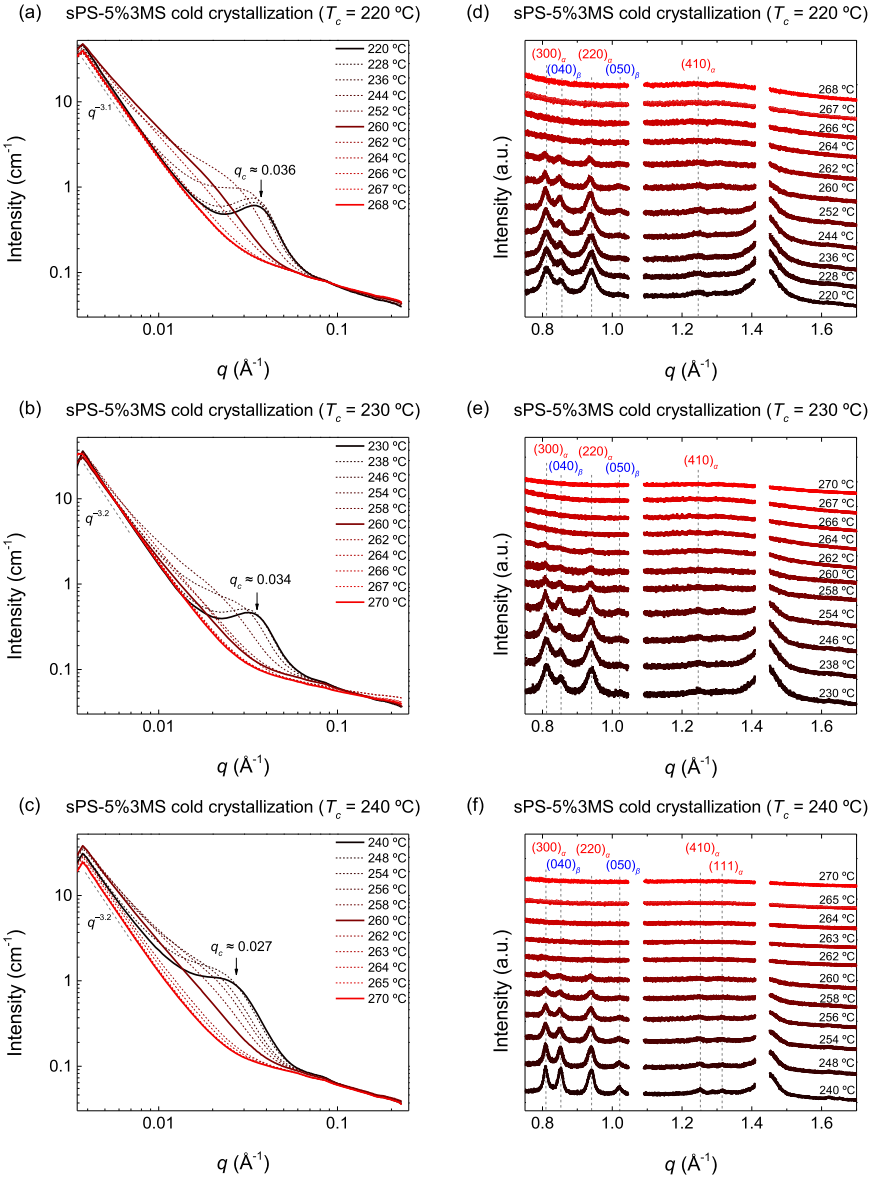

Figure 1. Simultaneous (a–c) SAXS and (d–f) WAXS heating profiles of sPS-5%3MS cold-crystallized specimens at a 2 °C min^{-1} rate. Black solid lines in the SAXS profiles refer to the starting profiles for each specimen at T_c, and the red solid lines denote the profiles of the molten state; dashed lines in the low q-region indicate the slope of the power-law decrease for molten state scattering, and all give the value of ca. 3. The WAXS profiles show that all give α-dominated crystals and the reflection peaks decrease gradually upon heating and completely melt after reaching ca. 265 °C without emerging new peaks.

reflections were calculated only for reflections in the q-range of 0.75–1.7 Å^{-1}.

RESULTS

Figure 1 shows the simultaneous SAXS/WAXS heating profiles of the cold-crystallized sPS-5%3MS specimen (T_c = 220, 230, and 240 °C) at a 2 °C min^{-1} rate. The black solid lines in SAXS profiles denote the initial scattering for each specimen, i.e., at temperatures of 200, 230, and 240 °C, respectively, for Figure 1a–c. Comparing these initial profiles, the lamellar peak position shifts from q_c = 0.036 to 0.027 Å^{-1}, corresponding to a long period (L_p) increase from L_p = 17 to 23 nm, i.e., a specimen cold-crystallized at higher temperatures exhibits greater interparticle distance between nanograins. Upon heating, the lamellar peak in each profile successively shifts to lower q positions and becomes broader, which represents the increase of L_p and the weakening of the nanograins' spatial correlation (i.e., structure factor). Finally, all of the SAXS profiles exhibit a power-law scattering profile $I(q) \sim q^P$ with P = −3.1 to −3.2 before reaching 270 °C, indicating that the molten state is of fractal structure with a fractal dimension of ca. 3. This applies to all current specimens of different comonomer contents (5–21 mol % 3MS) at molten state (cf. SI) as well as the molten state of the sPS homopolymer.[46,4746,47] Figure 1d–f shows the corresponding WAXS heating profiles, where the vertical dashed lines indicate the positions of characteristic reflections (indexed for each reflection plane) for each specimen at their T_c. As revealed by WAXS profiles, the cold-crystallized sPS-5%3MS specimens all exhibited an α-dominated structure, while a higher T_c results in sharper reflections, implying more perfect/ordered crystals formed at a higher T_c. Upon heating, the intensity of

https://dx.doi.org/10.1021/acs.macromol.9b01831
Macromolecules 2020, 53, 3059–3070

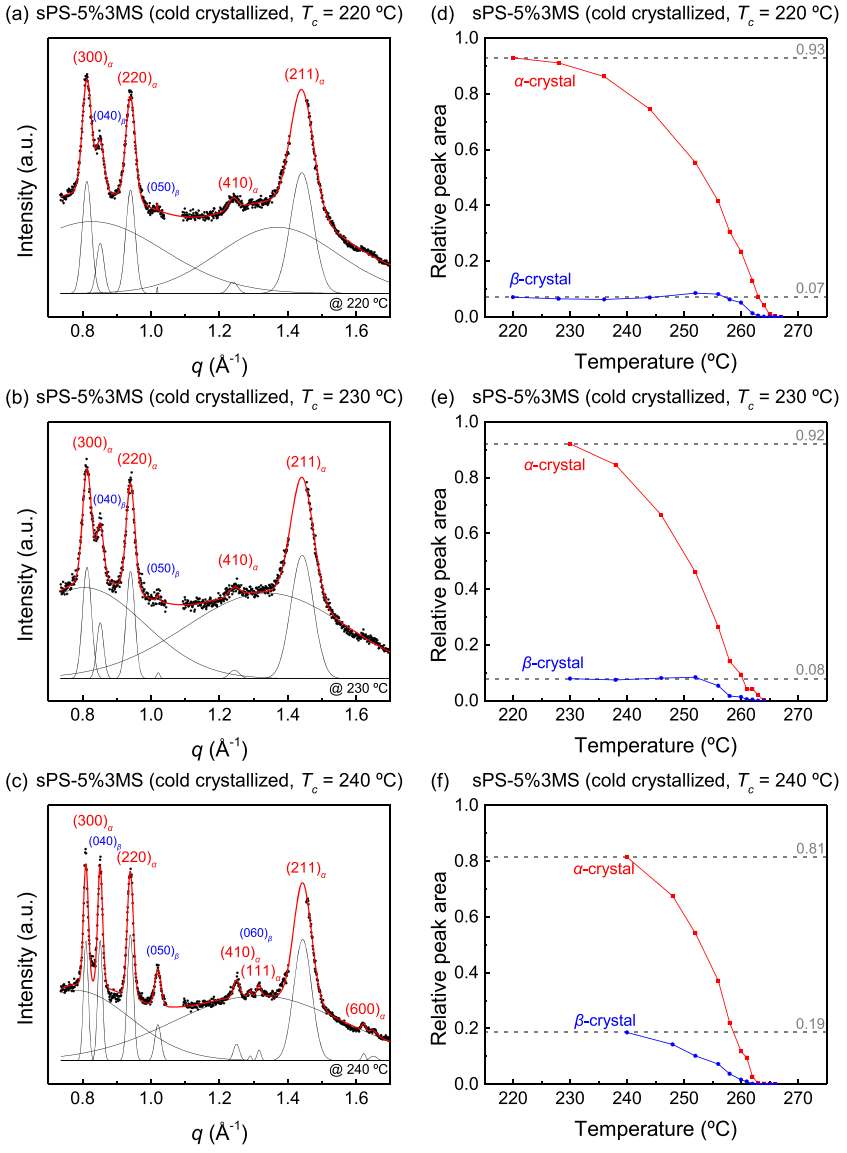

Figure 2. Representative peak-deconvolution WAXS profiles for sPS-5%3MS cold-crystallized specimens at temperatures of (a) 220 °C, (b) 230 °C, and (c) 240 °C. Black dots are the experimental profiles, and red lines are the fitting profiles that comprised two amorphous halos and crystalline reflection peaks (black solid line). (d)−(f) Evolutions of relative crystallinity between α and β crystals upon heating, and the values for each heating process are normalized with respect to the initial value. The WAXS profiles indicate that the α crystals always have a higher population than that of β crystals upon heating.

the reflections progressively decreases and finally gives amorphous halo profiles after reaching ca. 266 °C.

The evolution of the normalized relative crystallinity of α and β crystals upon heating is shown in Figure 2d−f, and the representative peak-deconvoluted WAXS profiles are illustrated in Figure 2a−c. It should be noted that, due to the instrumental setting for the in situ experiments, the q-range for the WAXS profile was limited to q = 0.72 − 1.7 Å^{-1}; hence, we consider only the relative crystallinity (the ratio of peak areas of α and β crystals, excluding the amorphous halo) here. Although there was a small amount of β crystals in the cold-crystallized sPS-5%3MS specimen, the α crystals remained as the dominant form up to melting. Upon heating, the crystalline area for all cases successively decreases without the emergence of any new reflections; thus, the heating process predominately reflects the melting behavior of α crystals. Among these different cold-crystallized temperatures, the initial relative amount of β crystals for each case increases from 0.07 to 0.19 with increasing cold crystallization temperature.

Figure 3 shows the SAXS heating profiles of sPS-5%3MS cold-crystallized specimens in the temperature range ca. 260−266 °C (before melting) with subtracting the contribution of the amorphous molten state. In this temperature region, the SAXS profiles contain majorly only the form factor scattering (insignificant contribution of the structure factor). To determine the shape of the nanograins, different form factor models have been tested (including a sphere, an ellipsoid, cylinder, a cylinder with a polydisperse length, and a cylinder with a polydisperse radius), and the shape of a cylinder with the polydisperse radius gives the best fit (cf. SI Model for SAXS Analysis). Thus, the solid lines presenting in Figure 3 are the fitting profiles using the form factor of the cylinder shape with a polydisperse radius, and the radius and length (thickness) of the cylindrical structure are summarized in Figure 4. As the temperature increases from 258 to 266 °C, the

https://dx.doi.org/10.1021/acs.macromol.9b01831
Macromolecules 2020, 53, 3059−3070

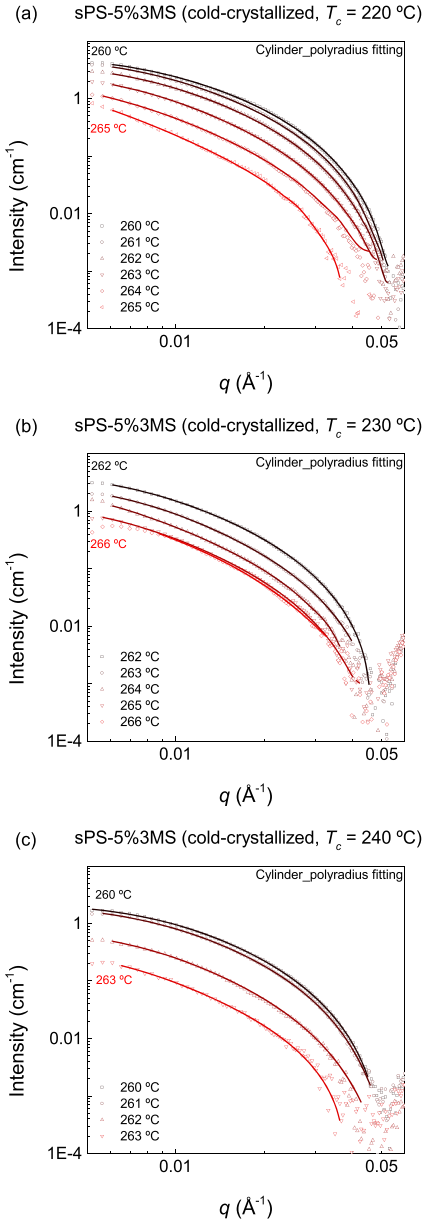

Figure 3. Reduced SAXS heating profiles of sPS-5%3MS cold-crystallized specimens at T_c of (a) 220 °C, (b) 230 °C, and (c) 240 °C before melting (ca. 260−266 °C), which gives mainly form factor scattering profiles after subtracting from the molten state profile. Solid lines are the fitting profiles using the cylindrical shape with a dispersed-radius form factor model.

radius generally increases from ca. 5 to 16 nm (Figure 4a) and the thickness (length) increases from ca. 13 to 16 nm (Figure 4b), indicating that the shape of the nanograins is close to a disk structure, which mostly grows in the lateral direction upon heating. Accordingly, the lamellar structure, which is assumed in the 1-D correlation function, cannot appropriately describe the profiles while approaching melting (cf. SI Model for SAXS Analysis). The reciprocal crystalline lamellar thickness ($1/l_c$) against the experimental temperature for sPS-5%3MS cold-crystallized specimens (that is α-dominated crystals) is plotted in Figure 5. With a gradual increase in the temperature, the melting line of crystals approaching the solid-melt equilibrium can be constructed by linearly extrapolating the reciprocal thickness points several degrees before complete melting (solid

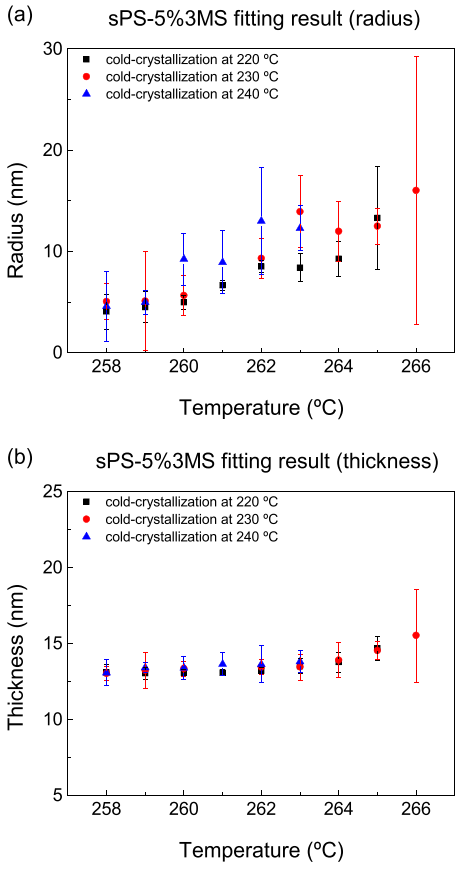

Figure 4. Evolution of (a) radius and (b) thickness of the nanograins during the heating scan, which is obtained from the reduced SAXS profiles fitting in Figure 3. Based on the fitting parameters, the nanograins are close to the disklike structure.

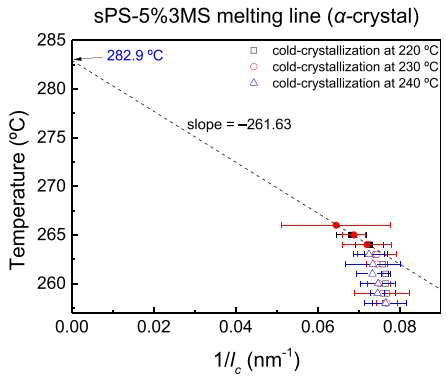

Figure 5. Evolution of the reciprocal crystal thickness ($1/l_c$) of sPS-5%3MS cold-crystallized specimens upon heating. The dashed line represents the melting line that is extrapolated linearly by the data points that are higher than 264 °C (solid symbols), giving the equilibrium melting temperature of sPS-5%3MS cold-crystallized α crystals as 282.9 ± 1.2 °C.

symbol, temperatures higher than 264 °C), which is represented in Figure 5 as a dashed line. Depending on the melting line, the equilibrium melting temperature (T_m°) for infinitely thick α crystals in the sPS-5%3MS system is 282.9 ± 1.2 °C.

Following the same approach, the melting lines of sPS-11%3MS, sPS-21%3MS, sPS-2%4MS, sPS-5%4MS, and sPS-10%4MS α crystals and the melting lines of sPS-5%3MS, sPS-

https://dx.doi.org/10.1021/acs.macromol.9b01831
Macromolecules 2020, 53, 3059−3070

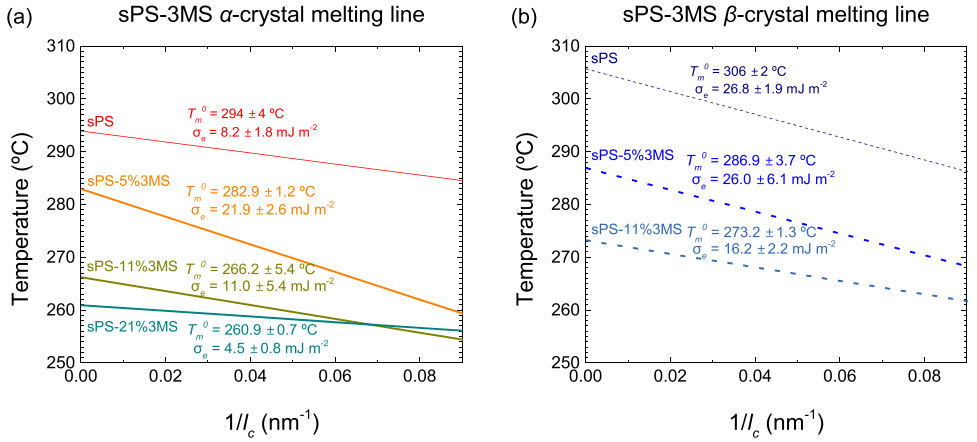

Figure 6. Equilibrium melting line for (a) α and (b) β crystals of the sPS homopolymer[39] and sPS-3MS random copolymers. The experimental data are removed from the figure for the sake of readability. Under the same comonomer contents, the β crystal always has a higher equilibrium melting temperature (T_m°) and a larger melting line slope (which corresponds to the fold surface energy, σ_e) than those of the α counterpart. For both α and β crystals, the σ_e decreases with increasing comonomer contents.

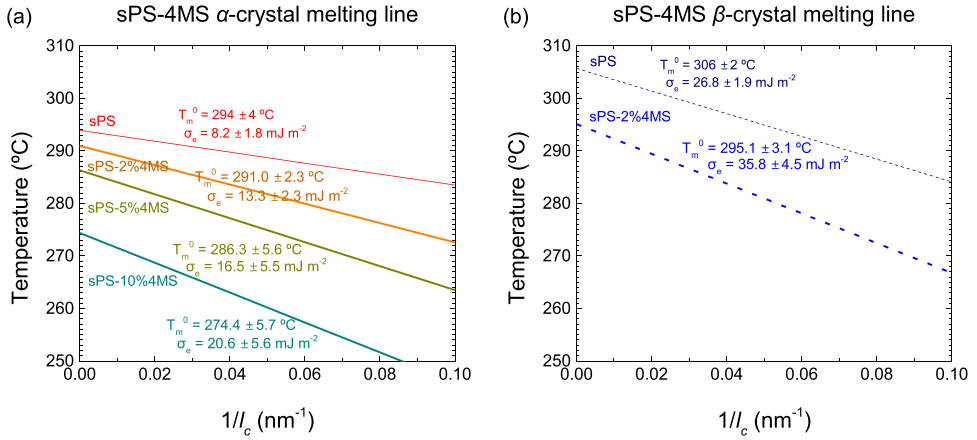

Figure 7. Equilibrium melting line for (a) α and (b) β crystals of the sPS homopolymer[39] and sPS-4MS random copolymers. The experimental data are removed from the figure for the sake of readability. Comparing the α and β crystals for the 2 mol % 4MS case, the β crystal has a higher equilibrium melting temperature (T_m°) and a larger melting line slope (which corresponds to the fold surface energy, σ_e) than those of the α counterpart. The σ_e in both α and β crystals increases with increasing comonomer contents.

11%3MS, and sPS-2%4MS β crystals were determined. The detailed analyses for these cases are shown in the Supporting Information. Figures 6 and 7 summarize the melting lines of α and β crystals of sPS-3MS and sPS-4MS series; the melting lines of the sPS homopolymer, determined in our previous report[39] using the Kratky−Porod approximation to extract the thickness information (cf. SI Model for SAXS Analysis), are also included. For better eligibility, the experimental data points were removed from these figures. For both α and β phases, equilibrium melting temperatures (T_m°) of the copolymers are all lower than the T_m° of the sPS homopolymer, and copolymers with higher comonomer contents would have lower T_m°. At a given comonomer level, the β crystal always has higher T_m° than that of the α crystal, indicating that the β phase remains the thermodynamically more stable structure (up to 11 mol % 3MS content and 2 mol % 4MS content).

DISCUSSION

Inclusion vs Exclusion. The polymorphism of sPS-3MS and sPS-4MS random copolymers after bulk thermal treatment (isothermal cold and melt crystallization) is reported previously.[40] These room-temperature WAXS profiles (cf. Figure 3, Tables 1 and 2 in ref 40) suggest that, except for the β structure of sPS-4MS, the comonomer units are at least partially incorporated into the α and β crystals in sPS-3MS and α crystals in sPS-4MS because of the larger unit cell parameters for copolymers than the parameters for homopolymers.[40] At elevated temperatures, these sPS random copolymers all have

Table 1. Summary of Equilibrium Melting Temperature (T_m°), Penalty Energy (Excess Energy, ε), and Fold Surface Energy (σ_e) of α Crystals for sPS-3MS and sPS-4MS Series, Which Were Obtained/Derived from Figures 6a and 7a[a]

	T_m° (x) (°C)	ε (MJ m^{-3})	σ_e (mJ m^{-2})
sPS[39]	294 ± 4		8.2 ± 1.8
sPS-5%3MS	282.9 ± 1.2	37.2 ± 4.0	21.9 ± 2.6
sPS-11%3MS	266.2 ± 5.4	42.4 ± 18.0	11.0 ± 5.4
sPS-21%3MS	260.9 ± 0.7	26.4 ± 2.4	4.5 ± 0.8
sPS-2%4MS	291.0 ± 2.3	21.7 ± 16.6	13.3 ± 2.3
sPS-5%4MS	286.3 ± 5.6	22.3 ± 16.2	16.5 ± 5.5
sPS-10%4MS	274.4 ± 5.7	28.3 ± 8.2	20.6 ± 5.6

[a]The corresponding values for the sPS homopolymer are obtained from the literature that used a similar approach.[39]

https://dx.doi.org/10.1021/acs.macromol.9b01831
Macromolecules 2020, 53, 3059−3070

Table 2. Summary of Equilibrium Melting Temperature (T_m°), Penalty Energy (Excess Energy, ε), and Fold Surface Energy (σ_e) of β Crystals for sPS-3MS and sPS-4MS Series, Which Were Obtained/Derived from Figures 6b and 7b[a]

	T_m° (x) (°C)	ε (MJ m^{-3})	σ_e (mJ m^{-2})
sPS[39]	306 ± 2		26.8 ± 1.9
sPS-5%3MS	286.9 ± 3.7	96.3 ± 18.5	26.0 ± 6.1
sPS-11%3MS	273.2 ± 1.3	75.1 ± 6.4	16.2 ± 2.2
sPS-2%4MS	295.1 ± 3.1	137.0 ± 39.5	35.8 ± 4.5

[a]The corresponding values for the sPS homopolymer are obtained from the literature that used a similar approach.[39]

greater crystal thickness (>10 nm for both α and β crystals) than that of the sPS homopolymer (<10 nm for both α and β crystals).[39] This observation might be expectable that, at the same crystallization temperature, introducing the comonomer units would depress the T_m° and then the supercooling for copolymers would decrease as well, which might give thicker crystals than those of the homopolymer case. Sanchez and Eby also gave theoretical expression to describe that the isothermal crystal thickness increases with increasing comonomer contents for both exclusion and inclusion models in an early report.[48] However, this concept is somehow controversial that Strobl et al. reported the thicknesses for the comonomer-excluded cases do not affect by the comonomer contents but only depend on the crystallization temperature,[7,22,28] and some suggested that the total exclusion case would lead to a thinner lamellar crystal morphology.[6,9,49] For the inclusion case, the Gibbs−Thomson plot in the report of Orts et al. showed that the crystal thickness increases with increasing comononer contents.[16] Although no systematic analyses of the crystal thickness between comonomer-excluded and comonomer-included cases for random copolymers have been reported yet, our experimental observations suggest that the comonomer units should be included in the crystalline structure.

Figure S47, Supporting Information (SI), shows the representative evolutions of $(300)_\alpha$ and $(040)_\beta$ reflections in sPS-5%3MS and sPS-2%4MS systems. Upon heating, both $(300)_\alpha$ and $(040)_\beta$ reflections shift linearly with temperature to lower q positions due to the thermal expansion of the lattice. When approaching melting, the $(300)_\alpha$ and $(040)_\beta$ reflection positions in sPS-5%3MS (Figure S47a,b) clearly deviate from the linear dependence and shift to much lower q values, showing abruptly increased a- and b-axes. For the sPS-2%4MS case, as illustrated in Figure S47c,d, although the shifting phenomena are not so apparent as the case of sPS-5%3MS due to its having lower comonomer contents, these still imply the weak tendency of lower-q shifting while approaching melting. These stronger lower-q shifting phenomena of the reflection peaks suggest that the lattice enlargement is beyond the thermal expansion, and the larger lattice size could reduce the steric effect, having a higher ability to incorporate more comonomer units. Thus, the larger crystalline thickness of these random copolymers and the lower-q shifting of the reflection peaks indicate that the comonomer units are not only partially included into the lattice but also could be incorporated more at elevated temperatures. Although the value of the comonomer concentration in the crystalline phase (x_c) is not exactly known, it is expected to approach the value (x) of bulk melt as a first approximation.

Penalty Energy and Fold Surface Energy Determination. The equilibrium melting temperature (T_m°), which can be determined by extrapolating the melting line to the case that l_c^{-1} approaches to 0 in the $l_c^{-1}-T$ plot, refers to the melting temperature of the infinite thick crystals. Thus, in the case of infinite thick crystals ($l_c^{-1} \sim 0$) for sPS-3MS and sPS-4MS random copolymers, the comonomer units are assumed to be fully incorporated into the crystalline structures, which gives $x_c \sim x$. Based on the fully incorporated assumption, the Sanchez−Eby equation in eq 4 can be reduced to

$$T_m^\circ(x) = T_m^\circ\left[1 - \frac{\varepsilon x}{\Delta H_m^\circ}\right] - \frac{2\sigma_e T_m^\circ}{\Delta H_m^\circ l_c} \tag{7}$$

where the first bracket at the right side describes the T_m° depression due to the incorporation of the comonomer units into the crystal and the second term at the right side describes the thickness dependence of the solid−liquid phase transition (i.e., the melting line). Thus, considering the T_m° depression of the infinite thick crystals where the contribution of fold surface energy (σ_e) can be neglected, the relationship of the equilibrium melting temperature between homopolymer T_m° and copolymer $T_m^\circ(x)$ is

$$T_m^\circ(x) + \frac{T_m^\circ \varepsilon x}{\Delta H_m^\circ} = T_m^\circ \tag{8}$$

and the penalty energy, ε, for uniformly incorporating the comonomer units in the crystalline structure would be

$$\Rightarrow \varepsilon = \frac{\Delta H_m^\circ (T_m^\circ - T_m^\circ(x))}{T_m^\circ x} \tag{9}$$

which is proportional to the level of melting temperature depression. After determining the value of ε from the level of equilibrium melting temperature depression for each copolymer system, the slope of the melting line, according to eq 7, can be defined as

$$\text{slope} = -\frac{2\sigma_e T_m^\circ}{\Delta H_m^\circ} \tag{10}$$

which represents the relation between the heat of fusion for the homopolymer (ΔH_m°) and the fold surface energy for the copolymer crystals (σ_e). Consequently, the σ_e for these random copolymers is

$$\Rightarrow \sigma_e = \frac{\Delta H_m^\circ(-\text{slope})}{2T_m^\circ} \tag{11}$$

Based on the derivations, the T_m°, ε, and σ_e for the sPS-3MS and sPS-4MS copolymers with different comonomer contents can be separately determined, and the results are summarized in Tables 1 (α crystals) and 2 (β crystals) (the corresponding values for the sPS homopolymer[39] are also included). It is to be noted that the ΔH_m° for the sPS homopolymer has been determined in a previous report where the ΔH_m° of α crystals is 82 ± 4 MJ m^{-3} and the ΔH_m° of β crystals is 146 ± 7 MJ m^{-3}.[39] (The ΔH_m° values for sPS-3MS and sPS-4MS random copolymers could not be used to determine the corresponding ε and σ_e, and the values are summarized in the SI.) At a given comonomer content, the ε values in β crystals are greater than the values in α crystals, which is consistent with the results of molecular mechanics calculations[40] that incorporating comonomer units into the β lattice gives higher energy increase than incorporating comonomer units into α crystals.

Penalty Energy. The T_m° depression of sPS α and β crystals after incorporating different levels of 3MS or 4MS comonomer

https://dx.doi.org/10.1021/acs.macromol.9b01831
Macromolecules 2020, 53, 3059−3070

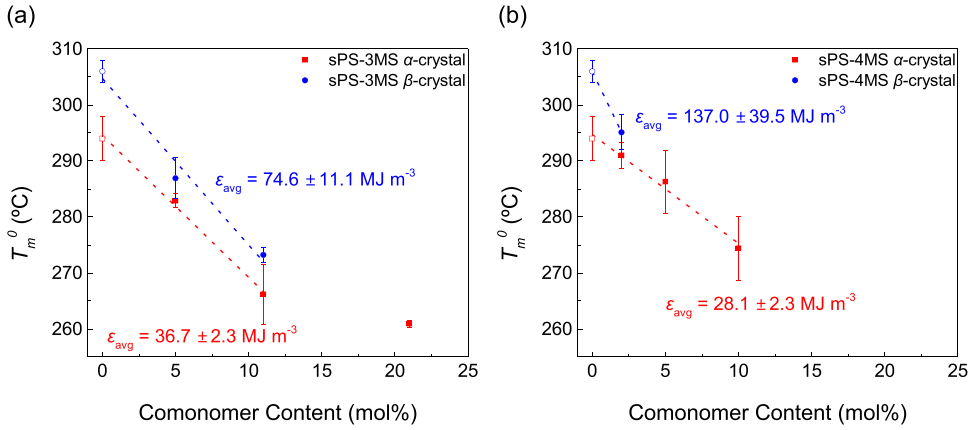

Figure 8. Relation between the comonomer content and the equilibrium melting temperature (T_m°). Red symbols represent α crystals, and the blue symbols represent β crystals. (a) For the 3MS case, the T_m° shows a linear dependence on comonomer contents up to 11 mol % 3MS for both α and β crystals but deviates at higher comonomer levels (21 mol %). (b) For the 4MS case, the T_m° shows a linear dependence on both α and β crystals. This linearity indicates that the penalty energy for incorporating comonomer units within this range is nearly a constant.

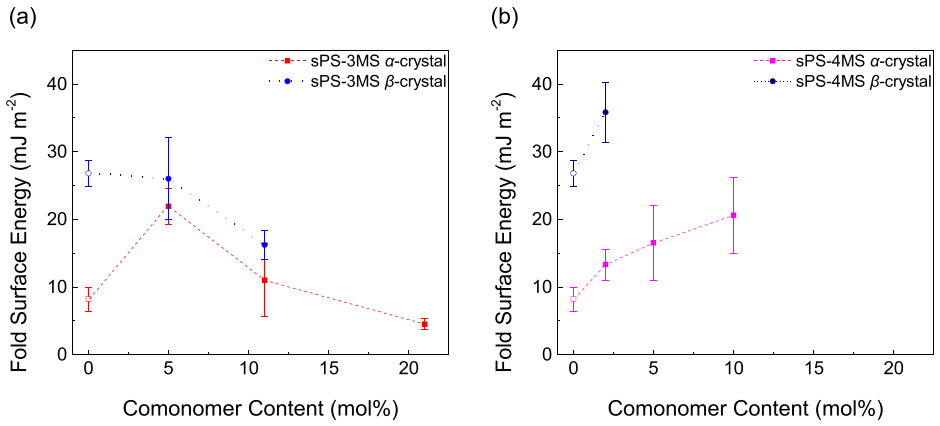

Figure 9. Relation between the comonomer content and the fold surface energy (σ_e). Red symbols represent α crystals, and the blue symbols represent β crystals. (a) In sPS-3MS series, the σ_e of the α structure increases first for the homopolymer case to 5 mol % 3MS content and then decreases with increasing 3MS contents; the σ_e of the β structure decreases with increasing 3MS content. (b) In sPS-4MS series, the σ_e of both α and β structure increases with increasing 4MS content.

units is illustrated in Figure 8, in which red squares indicate the α phase and the blue circles indicate the β phase, whereas the sPS homopolymer cases are indicated as open symbols and solid symbols for sPS-3MS and sPS-4MS, respectively. In Figure 8a, after incorporating 3MS units into crystals, the relation between T_m° and the comonomer content is linear in the low 3MS content range (up to 11 mol %) for both α and β crystals, but a deviation from the linear dependence is observed at a higher 3MS level (21 mol %) for α crystals; from the linear fitting (marked by the dashed line in the figure) within the low 3MS content range, the average penalty energy (ε_{avg}) for the incorporation of 3MS units is 36.7 ± 2.3 MJ m^{-3} for the α lattice and 74.6 ± 11.1 MJ m^{-3} for the β lattice. In Figure 8b, after incorporating 4MS units into crystals, the relation between T_m° and comonomer contents is also linear for α crystals up to 10 mol % 4MS (marked by the dashed line in the figure) and gives average penalty energy (ε_{avg}) of 28.1 ± 2.3 MJ m^{-3} for α crystals. As for the β lattice, as only 2 mol % 4MS content can form β crystals and the average penalty energy (ε_{avg}) for β crystals is estimated with large error bounds as 137.0 ± 39.5 MJ m^{-3}. Generally, the β structure has larger ε than that of the α structure, reflecting that the high-symmetry close-packed β structure has less comonomer compatibility than the more loosely packed α structure. The observed linearity indicates that the penalty energy for incorporating each comonomer unit into the α or β structure at low comonomer concentration ranges is nearly a constant, consistent with the notion that the structure is only locally distorted to accommodate these impurities without mutual interaction between comonomer units or significant breaking of the crystalline symmetry. However, after exceeding a certain threshold comonomer content (above 11 mol % 3MS units or 2 mol % 4MS units), sPS-21%3MS, sPS-5%4MS, and sPS-10%4MS cannot form the β structure but form the α-dominated structure, indicating that the β structure could not accommodate these amounts of impurities without strongly increasing the structural energy, making the β structure less favorable than the α structure.[40] As for the α structure, it is already loosely packed to start with, and the unit cell volume increases with the comonomer content[40] to reduce the steric repulsion, hence resulting in smaller values of ε.

Note that the ε value for α-crystals with a 21 mol % 3MS content deviates clearly from the linear relationship. Previous studies on poly(β-hydroxybutyrate-*co*-β-hydroxyvalerate),[16,50] poly(ethylene-*co*-1-octene),[17] and poly(ethylene terephthalate-*co*-2,6-dicarboxylate)[14] also showed decreasing ε with increas-

https://dx.doi.org/10.1021/acs.macromol.9b01831
Macromolecules 2020, 53, 3059−3070

ing comonomer content. These observations of decreasing ε at higher comonomer levels imply that the comonomer inclusion is more favored at higher comonomer content levels, consistent with the correspondingly reported distorted lattice after incorporating excessive comonomer units. All of these observations over concentration dependence of ε signify that there can be interactions among comonomer units at higher comonomer levels; ε can only be viewed as a constant only at lower comonomer contents.

Furthermore, sPS-3MS α-crystals have larger ε_{avg} than that of sPS-4MS α-crystals, and sPS-4MS β-crystals have larger ε_{avg} than that of sPS-3MS β-crystals. These results indicate that for α-crystals the structure can tolerate the 4MS units more than the 3MS units; for β crystals, incorporating the 4MS units into the β structure has a higher energy increase than that of incorporating the 3MS units. These theoretical analyses agree with the results of molecular mechanics computation in our previous report that, at fixed lattice size, incorporating 3MS units into the α structure has a stronger energy increase than that of incorporating 4MS units and the situation inverses for the β structure; the β structure has a more significant energy increase than that of the α structure after comonomer incorporation[40] (cf. SI α and β structures). Therefore, the suppression of the β crystal formation is because of the higher ε that renders the β structure less favorable; this is especially clear for the sPS-4MS series.

Fold Surface Energy. Figure 9 shows the respective fold surface energy (σ_e) in sPS-3MS and sPS-4MS series, as summarized in Tables 1 and 2. In the sPS-3MS series (Figure 9a), the σ_e of the random copolymers (both α and β crystals) all decreases with increasing comonomer content; however, for the sPS-3MS α crystals, the σ_e first increases from 0 mol % content (homopolymer) to 5 mol % content. In sPS-4MS series (Figure 9b), the σ_e increases with the 4MS contents in both α and β crystals. For the comonomer inclusion case, the decrease of σ_e with increasing comonomer content was also reported in the polyethylene random copolymer case.[15] These observations are different from the comonomer exclusion cases reported by Strobl et al.[7,22,28] that the σ_e is independent of the comonomer content.

As crystals with higher σ_e value would have a higher tendency to thicken to reduce the contribution of σ_e that could further lower the total free energy of the crystal,[51] the σ_e can be viewed as the indicator of the thickening tendency. For the sPS homopolymer, the β phase has a greater σ_e value than that of the α phase.[39] However, after incorporating the 3MS units, the σ_e of the α crystal increases first (from the homopolymer to the 5 mol % 3MS content) and then decreases. The reason for the σ_e increases in the sPS-5%3MS α crystal could be that the α crystal is a loosely packed structure; therefore, after incorporating a very small amount of comonomer units, the penalty energy increase in the α crystal is less than that in the β crystal, and this ε increase could be somehow compensated by thickening, giving a larger σ_e value than that of the α crystal in the sPS homopolymer case. On the other hand, higher ε in the β crystal is relatively harder to be compensated by thickening; thus, incorporating more 3MS units leads to lower σ_e in the β crystal. With increasing 3MS content, the effect of this kind of compensation becomes insignificant and reduces the tendency for thickening, which expresses by the value of σ_e.

In contrast, for the sPS-4MS series, the σ_e value of α crystals increases with increasing 4MS content. Depending on the penalty energy of α crystals between 3MS and 4MS unit, incorporating 4MS units have less energy increase than that of 3MS units (incorporating 4MS units into the α structure is relatively favored than incorporating 3MS units), so the compensation ability of sPS-4MS is higher than that of sPS-3MS systems, giving the increasing relation between σ_e and 4MS content. Hence, within the 10 mol % 4MS content, the more the incorporated comonomer units, the stronger the tendency toward crystal thickening, leading to a higher σ_e value. Nevertheless, the energy increase for incorporating more 4MS units would make this compensation effect less significant. Following this argument, the σ_e value for sPS-4MS α crystals should also decrease after reaching a certain amount of 4MS incorporation (more than the 10 mol % 4MS content); this, however, is not observed within the limit of the 10 mol % 4MS content. For the β crystal, the σ_e of the 2 mol % 4MS content is larger than the value in the homopolymer case. Although incorporating 4MS units into the β structure has greater penalty energy than that of incorporating 3MS units, the result suggests that the energy increase can be compensated by thickening due to the very small amount of 4MS units.

CONCLUSIONS

The equilibrium melting temperature (T_m°), determined via the Gibbs−Thomson approach, of α and β crystals for the random copolymers shows that the T_m° decreases with increasing comonomer levels. The β crystal always has a higher T_m° than that of the α counterpart, indicating that the β phase remains the thermodynamically stable structure. The T_m° depression is quantitatively analyzed within the Sanchez−Eby theoretical framework with the approximation that the comonomer units are almost fully incorporated into the crystalline lattice when approaching final melting. The penalty energy (ε) for the β structure is more significant than that for the α structure, which implies that the more densely packed β lattice is more reluctant to accommodate the comonomer units. The ε value for the β crystals to accommodate 4MS units is higher than that for accommodating 3MS units; the trend is reversed for α crystals, consistent with our previous results of molecular mechanics computation. In the case of low comonomer contents (up to ca. 10 mol %), the ε value is nearly constant and can be represented by a mean value ε_{avg}, indicating that these comonomer units can be considered as randomly incorporated without significant interactions. Further increased incorporation of comonomer units leads to a decreased ε value, presumably due to the inevitable interactions and structural distortion.

ASSOCIATED CONTENT

Supporting Information

The Supporting Information is available free of charge at https://pubs.acs.org/doi/10.1021/acs.macromol.9b01831.

Model for SAXS analysis; equilibrium melting temperature analyses for the sPS-11%3MS α crystal, sPS-21%3MS α crystal, sPS-5%3MS β crystal, sPS-11%3MS β crystal, sPS-2%4MS α crystal, sPS-5%4MS α crystal, sPS-10%4MS α crystal, and sPS-2%4MS β crystal; equilibrium heat of fusion (ΔH_m°); evolution of peak position upon heating; α and β structures (molecular mechanics computation); and α'' form in sPS-4MS (PDF)

https://dx.doi.org/10.1021/acs.macromol.9b01831
Macromolecules 2020, 53, 3059−3070

AUTHOR INFORMATION

Corresponding Authors

Po-Hsun Chen − *Department of Chemical Engineering, National Tsing Hua University, Hsinchu 30013, Taiwan;* orcid.org/0000-0002-3670-8241; Email: zero00023@gapp.nthu.edu.tw

An-Chung Su − *Department of Chemical Engineering, National Tsing Hua University, Hsinchu 30013, Taiwan*; Email: acsu@mx.nthu.edu.tw

Authors

Shi-Jie Lin − *Department of Chemical Engineering, National Tsing Hua University, Hsinchu 30013, Taiwan*

Jing-Cherng Tsai − *Department of Chemical Engineering, National Chung Cheng University, Chiayi 62102, Taiwan*

U-Ser Jeng − *Department of Chemical Engineering, National Tsing Hua University, Hsinchu 30013, Taiwan; National Synchrotron Radiation Research Center, Hsinchu 30076, Taiwan;* orcid.org/0000-0002-2247-5061

Complete contact information is available at: https://pubs.acs.org/10.1021/acs.macromol.9b01831

Notes

The authors declare no competing financial interest.

ACKNOWLEDGMENTS

Financial support from the Ministry of Science and Technology (MoST 101-2221-E-007-037-MY3) is gratefully acknowledged. Thanks are also due to team members of TLS BL23A, NSRRC for beamline alignment and technical support. Comments from the anonymous referees are much appreciated, which helps us to check the analytical application of the Sanchez−Eby theory.

REFERENCES

(1) Sanchez, I. C.; Eby, R. K. Thermodynamics and Crystallization of Random Copolymers. *Macromolecules* **1975**, *8*, 638−641.

(2) Flory, P. J. Theory of Crystallization in Copolymers. *Trans. Faraday Soc.* **1955**, *51*, No. 848.

(3) Richardson, M. J.; Flory, P. J.; Jackson, J. B. Crystallization and Melting of Copolymers of Polymethylene. *Polymer* **1963**, *4*, 221−236.

(4) Alamo, R. G.; Viers, B. D.; Mandelkern, L. Phase Structure of Random Ethylene Copolymers: A Study of Counit Content and Molecular Weight as Independent Variables. *Macromolecules* **1993**, *26*, 5740−5747.

(5) Chen, H. Y.; Chum, S. P.; Hiltner, A.; Baer, E. Comparison of Semicrystalline Ethylene−styrene and Ethylene−octene Copolymers Based on Comonomer Content. *J. Polym. Sci., Part B: Polym. Phys.* **2001**, *39*, 1578−1593.

(6) Obi, B. E.; DeLassus, P.; Grulke, E. A. Model for the Solid-Liquid Phase Transitions (Melting) of Undiluted Random Semicrystalline Copolymers of Vinylidene Chloride with Methyl Acrylate Monomers. *Macromolecules* **1994**, *27*, 5491−5497.

(7) Hauser, G.; Schmidtke, J.; Strobl, G. The Role of Co-Units in Polymer Crystallization and Melting: New Insights from Studies on Syndiotactic Poly(propene-co-octene). *Macromolecules* **1998**, *31*, 6250−6258.

(8) Crist, B.; Williams, D. N. Crystallization and Melting of Model Ethylene-Butene Random Copolymers: Thermal Studies. *J. Macromol. Sci., Part B: Phys.* **2000**, *39*, 1−13.

(9) Crist, B.; Howard, P. R. Crystallization and Melting of Model Ethylene−Butene Copolymers. *Macromolecules* **1999**, *32*, 3057−3067.

(10) Huang, J.; Lisowski, M. S.; Runt, J.; Hall, E. S.; Kean, R. T.; Buehler, N.; Lin, J. S. Crystallization and Microstructure of Poly(l-lactide-co-meso-lactide) Copolymers. *Macromolecules* **1998**, *31*, 2593−2599.

(11) Crist, B.; Finerman, T. M. Copolymer Crystallization: Approaching Equilibrium. *Polymer* **2005**, *46*, 8745−8751.

(12) Goldbeck-Wood, G. On the Melting-Point Depression of Copolymer Crystals. *Polymer* **1992**, *33*, 778−782.

(13) Crist, B. Thermodynamics of Statistical Copolymer Melting. *Polymer* **2003**, *44*, 4563−4572.

(14) Wendling, J.; Suter, U. W. A New Model Describing the Cocrystallization Behavior of Random Copolymers. *Macromolecules* **1998**, *31*, 2516−2520.

(15) Martinez-Salazar, J.; Cuesta, M. S.; Calleja, F. J. B. Equilibrium and Non-equilibrium Melting of Branched Polyethylene Relating to Defect Incorporation within Crystals. *Colloid Polym. Sci.* **1987**, *265*, 239−245.

(16) Orts, W. J.; Marchessault, R. H.; Bluhm, T. L. Thermodynamics of the Melting Point Depression in Poly(β-hydroxybutyrate-co-β-hydroxyvalerate) Copolymers. *Macromolecules* **1991**, *24*, 6435−6438.

(17) Kim, M.-H.; Phillips, P. J.; Lin, J. S. The Equilibrium Melting Points of Random Ethylene-Octene Copolymers: A Test of the Flory and Sanchez−Eby Theories. *J. Polym. Sci., Part B: Polym. Phys.* **2000**, *38*, 154−170.

(18) Pérez-Camargo, R. A.; Arandia, I.; Safari, M.; Cavallo, D.; Lotti, N.; Soccio, M.; Müller, A. J. Crystallization of Isodimorphic Aliphatic Random Copolyesters: Pseudo-eutectic Behavior and Double-Crystalline Materials. *Eur. Polym. J.* **2018**, *101*, 233−247.

(19) Yu, Y.; Wei, Z.; Liu, Y.; Hua, Z.; Leng, X.; Li, Y. Effect of Chain Length of Comonomeric Diols on Competition and Miscibility of Isodimorphism: A Comparative Study of Poly(butylene glutarate-co-butylene azelate) and Poly(octylene glutarate-co-octylene azelate). *Eur. Polym. J.* **2018**, *105*, 274−285.

(20) Papageorgiou, G. Z.; Bikiaris, D. N. Synthesis and Properties of Novel Biodegradable/Biocompatible Poly[propylene-co-(ethylene succinate)] Random Copolyesters. *Macromol. Chem. Phys.* **2009**, *210*, 1408−1421.

(21) Terzopoulou, Z.; Tsanaktsis, V.; Bikiaris, D. N.; Exarhopoulos, S.; Papageorgiou, D. G.; Papageorgiou, G. Z. Biobased Poly(ethylene furanoate-co-ethylene succinate) Copolyesters: Solid State Structure, Melting Point Depression and Biodegradability. *RSC Adv.* **2016**, *6*, 84003−84015.

(22) Heck, B.; Hugel, T.; Iijima, M.; Sadiku, E.; Strobl, G. Steps in the Transition of an Entangled Polymer Melt to the Partially Crystalline State. *New J. Phys.* **1999**, *1*, 1−17.

(23) Iijima, M.; Strobl, G. Isothermal Crystallization and Melting of Isotactic Polypropylene Analyzed by Time- and Temperature-Dependent Small-Angle X-ray Scattering Experiments. *Macromolecules* **2000**, *33*, 5204−5214.

(24) Fu, Q.; Heck, B.; Strobl, G.; Thomann, Y. A Temperature-and Molar Mass-dependent Change in the Crystallization Mechanism of Poly(1-butene): Transition from Chain-folded to Chain-extended Crystallization? *Macromolecules* **2001**, *34*, 2502−2511.

(25) Al-Hussein, M.; Strobl, G. The Melting Line, the Crystallization Line, and the Equilibrium Melting Temperature of Isotactic Polystyrene. *Macromolecules* **2002**, *35*, 1672−1676.

(26) Cho, T.-Y.; Strobl, G. Temperature Dependent Variations in the Lamellar Structure of Poly(L-lactide). *Polymer* **2006**, *47*, 1036−1043.

(27) Strobl, G. Crystallization and Melting of Bulk Polymers: New Observations, Conclusions and a Thermodynamic Scheme. *Prog. Polym. Sci.* **2006**, *31*, 398−442.

(28) Cho, T. Y.; Heck, B.; Strobl, G. Equations Describing Lamellar Structure Parameters and Melting Points of Polyethylene-co-(butene/octene)s. *Colloid Polym. Sci.* **2004**, *282*, 825−832.

(29) Greis, O.; Xu, Y.; Asano, T.; Petermann, J. Morphology and Structure of Syndiotactic Polystyrene. *Polymer* **1989**, *30*, 590−594.

(30) Guerra, G.; Vitagliano, V. M.; De Rosa, C.; Petraccone, V.; Corradini, P. Polymorphism in Melt Crystallized Syndiotactic Polystyrene Samples. *Macromolecules* **1990**, *23*, 1539−1544.

(31) De Rosa, C.; Rapacciuolo, M.; Guerra, G.; Petraccone, V.; Corradini, P. On the Crystal Structure of the Orthorhombic Form of Syndiotactic Polystyrene. *Polymer* **1992**, *33*, 1423−1428.
(32) Chatani, Y.; Shimane, Y.; Ijitsu, T.; Yukinari, T. Structural Study on Syndiotactic Polystyrene: 3. Crystal Structure of Planar Form I. *Polymer* **1993**, *34*, 1625−1629.
(33) Corradini, P.; De Rosa, C.; Guerra, G.; Napolitano, R.; Petraccone, V.; Pirozzi, B. Conformational and Packing Energy of the Crystalline α Modification of Syndiotactic Polystyrene. *Eur. Polym. J.* **1994**, *30*, 1173−1177.
(34) Manfredi, C.; De Rosa, C.; Guerra, G.; Rapacciuolo, M.; Auriemma, F.; Corradini, P. Structural Changes Induced by Thermal Treatments on Emptied and Filled Clathrates of Syndiotactic Polystyrene. *Macromol. Chem. Phys.* **1995**, *196*, 2795−2808.
(35) De Rosa, C. Crystal Structure of the Trigonal Modification (α form) of Syndiotactic Polystyrene. *Macromolecules* **1996**, *29*, 8460−8465.
(36) Cartier, L.; Okihara, T.; Lotz, B. The α'' "Superstructure" of Syndiotactic Polystyrene: A Frustrated Structure. *Macromolecules* **1998**, *31*, 3303−3310.
(37) Woo, E. M.; Sun, Y. S.; Yang, C. P. Polymorphism, Thermal Behavior, and Crystal Stability in Syndiotactic Polystyrene vs. Its Miscible Blends. *Prog. Polym. Sci.* **2001**, *26*, 945−983.
(38) Sun, Y. S.; Woo, E. M. Morphology and Crystal Structure of Cold-Crystallized Syndiotactic Polystyrene. *Polymer* **2001**, *42*, 2241−2245.
(39) Su, C. H.; Jeng, U.; Chen, S. H.; Cheng, C. Y.; Lee, J. J.; Lai, Y. H.; Su, W. C.; Tsai, J. C.; Su, A. C. Thermodynamic Characterization of Polymorphs in Bulk-Crystallized Syndiotactic Polystyrene via Small/Wide-Angle X-ray Scattering and Differential Scanning Calorimetry. *Macromolecules* **2009**, *42*, 4200−4207.
(40) Chen, P.-H.; Lan, Y.-K.; Lin, S.-J.; Tsai, J.-C.; Jeng, U. S.; Su, A.-C. Crystallization of α versus β Phases in Syndiotactic Poly(styrene-stat-3-methylstyrene) and Poly(styrene-stat-4-methylstyrene). *ACS Appl. Polym. Mater.* **2019**, *1*, 251−258.
(41) Manfredi, C.; Guerra, G.; De Rosa, C.; Busico, V.; Corradini, P. Effects of p-Methylstyrene Comonomeric Units on the Polymorphic Behavior of Syndiotactic Polystyrene. *Macromolecules* **1995**, *28*, 6508−6515.
(42) De Rosa, C.; Buono, A.; Ricci, A.; De Luca, F.; Caporaso, L. Polymorphic Behavior of Copolymers of Syndiotactic Polystyrene with m-Methylstyrene. *Macromolecules* **2003**, *36*, 6389−6400.
(43) Chen, Y.-P.; Tsai, J.-C.; Hong, J.-L. Novel Complex Catalyst of η3-(Pentamethylcyclopentadienyl) dimethylaluminum/Titanium (IV) Butoxide (Cp* AlMe2/Ti (OBu) 4) for Syndiotactic Polystyrene. *J. Chin. Chem. Soc.* **2003**, *50*, 205−210.
(44) Jeng, U.-S.; Su, C. H.; Su, C.-J.; Liao, K.-F.; Chuang, W.-T.; Lai, Y.-H.; Chang, J.-W.; Chen, Y.-J.; Huang, Y.-S.; Lee, M.-T.; et al. A Small/Wide-Angle X-Ray Scattering Instrument for Structural Characterization of Air−Liquid Interfaces, Thin Films and Bulk Specimens. *J. Appl. Crystallogr.* **2010**, *43*, 110−121.
(45) NIST Model Functions Help File. ftp://ftp.ncnr.nist.gov/pub/sans/kline/Download/SANS_Model_Docs_v4.10.pdf (accessed, 2014).
(46) Su, C. H.; Jeng, U.; Chen, S. H.; Lin, S. J.; Wu, W. R.; Chuang, W.-T.; Tsai, J. C.; Su, A. C. Nanograin Evolution in Cold Crystallization of Syndiotactic Polystyrene As Illustrated via in Situ Small/Wide-Angle X-ray Scattering and Differential Scanning Calorimetry. *Macromolecules* **2009**, *42*, 6656−6664.
(47) Su, C.-H.; Wu, W.-R.; Chen, C.-Y.; Su, C.-J.; Chuang, W.-T.; Liao, K.-F.; Chen, S.-H.; Su, A.-C.; Jeng, U.-S. Nanograin Nucleation at the Growth Front in Melt Crystallization of Syndiotactic Polystyrene. *Polymer* **2016**, *105*, 414−421.
(48) Sanchez, I. C.; Eby, R. K. Crystallization of Random Copolymers. *J. Res. Natl. Bur. Stand., Sect. A* **1973**, *77A*, No. 353.
(49) Crist, B.; Mirabella, F. M. Crystal Thickness Distributions from Melting Homopolymers or Random Copolymers. *J. Polym. Sci., Part B: Polym. Phys.* **1999**, *37*, 3131−3140.
(50) Wendling, J.; Suter, U. W. On the Isomorphism of Poly(β-hydroxybutyrate-co-β-hydroxyvalerate) Random Copolymers. *Macromol. Theory Simul.* **1999**, *8*, 110−118.
(51) Sanchez, I. C.; Colson, J. P.; Eby, R. K. Theory and Observations of Polymer Crystal Thickening. *J. Appl. Phys.* **1973**, *44*, 4332−4339.

https://dx.doi.org/10.1021/acs.macromol.9b01831
Macromolecules 2020, 53, 3059−3070